Inorganic Chemistry

Article

pubs.acs.org/IC

Saturation Kinetics in Phenolic O–H Bond Oxidation by a Mononuclear Mn(III)–OH Complex Derived from Dioxygen

Gayan B. Wijeratne, Briana Corzine, Victor W. Day, and Timothy A. Jackson*

[†]Department of Chemistry and Center for Environmentally Beneficial Catalysis, University of Kansas, Lawrence, Kansas 66045, United States

Supporting Information

ABSTRACT: The mononuclear hydroxomanganese(III) complex, $[Mn^{III}(OH)(dpaq)]^+$, which is supported by the amide-containing N_5 ligand dpaq (dpaq = 2-[bis(pyridin-2-ylmethyl)]amino-*N*-quinolin-8-yl-acetamidate) was generated by treatment of the manganese(II) species, $[Mn^{II}(dpaq)](OTf)$, with dioxygen in acetonitrile solution at 25 °C. This oxygenation reaction proceeds with essentially quantitative yield (greater than 98% isolated yield) and represents a rare example of an O_2-mediated oxidation of a manganese(II) complex to generate a single product. The X-ray diffraction structure of $[Mn^{III}(OH)(dpaq)]^+$ reveals a short Mn–OH distance of 1.806(13) Å, with the hydroxo moiety *trans* to the amide function of the dpaq ligand. No shielding of the hydroxo group is observed in the solid-state structure. Nonetheless, $[Mn^{III}(OH)(dpaq)]^+$ is remarkably stable, decreasing in concentration by only 10% when stored in MeCN at 25 °C for 1 week. The $[Mn^{III}(OH)(dpaq)]^+$ complex participates in proton-coupled electron transfer reactions with substrates with relatively weak O–H and C–H bonds. For example, $[Mn^{III}(OH)(dpaq)]^+$ oxidizes TEMPOH (TEMPOH = 2,2′-6,6′-tetramethylpiperidine-1-ol), which has a bond dissociation free energy (BDFE) of 66.5 kcal/mol, in MeCN at 25 °C. The hydrogen/deuterium kinetic isotope effect of 1.8 observed for this reaction implies a concerted proton–electron transfer pathway. The $[Mn^{III}(OH)(dpaq)]^+$ complex also oxidizes xanthene (C–H BDFE of 73.3 kcal/mol in dimethylsulfoxide) and phenols, such as 2,4,6-tri-*t*-butylphenol, with BDFEs of less than 79 kcal/mol. Saturation kinetics were observed for phenol oxidation, implying an initial equilibrium prior to the rate-determining step. On the basis of a collective body of evidence, the equilibrium step is attributed to the formation of a hydrogen-bonding complex between $[Mn^{III}(OH)(dpaq)]^+$ and the phenol substrates.

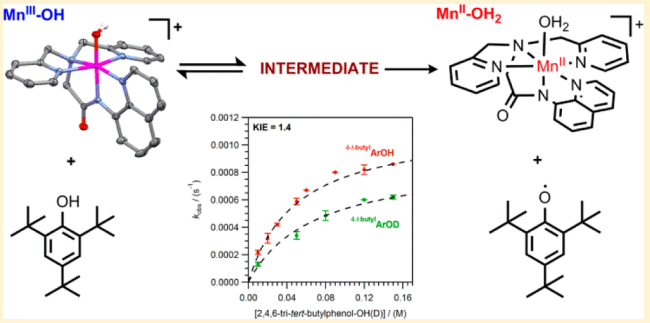

INTRODUCTION

Manganese-dependent enzymes play diverse biological roles, ranging from the generation of deoxynucleotides in pathogenic bacteria,[1] to the water splitting reaction of plants, algea, and cyanobacteria.[2] Hydroxo-manganese adducts have been proposed to play critical roles in the catalytic cycles of a small, yet diverse, set of these manganese-dependent enzymes.[2−6] For example, experimental[7] and computational[8,9] studies have provided strong support for a mononuclear hydroxomanganese(III), Mn^{III}–OH, adduct in the oxidized state of manganese-superoxide dismutase (MnSOD). This enzyme catalyzes the disproportionation of superoxide to dioxygen and hydrogen peroxide, thereby defending aerobic organisms from a reactive oxygen species.[3,4] The Mn^{III}–OH unit of oxidized MnSOD is involved in a hydrogen-bonding network with a nearby glutamine residue that plays a controlling role in the functionally important redox-tuning mechanism of the enzyme.[10−12]

There is also evidence for hydroxo-manganese species in the active sites of Mn-lipoxygenase[13] and the oxygen-evolving complex (OEC).[14,15] These enzymes respectively catalyze the dioxygenation of polyunsaturated fatty acids[5,6] and water splitting.[2] For both Mn-lipoxygenase and the OEC, hydroxo-manganese species have been proposed to participate in proton-coupled electron-transfer (PCET) reactions.[16,17] Support for a concerted proton–electron transfer (CPET) reaction in Mn-lipoxygenase comes from the fact that the conversion of α-linoleic acid to its hydroperoxy-derivative proceeds with a temperature-independent[18] kinetic isotope effect (KIE; k_H/k_D) of 20–24.[6] For the OEC, the proposition that a hydroxo-manganese species participates in catalytically relevant PCET is more tenuous, as there is substantial debate regarding the mechanistic details of this system.[2,19−23] Nonetheless, the abstraction of a hydrogen-atom from a hydroxo- or aqua-manganese moiety by a nearby tyrosyl radical, $Y_zO\bullet$, has been proposed as one of several possible mechanisms for stepwise oxidation of the tetramanganese cluster during turnover.[24−26] Terminal water ligands and bridging hydroxide ligands in dimanganese(III,III), dimanganese(III,IV), and dimanganese(IV,IV) model complexes have O–H bond dissociation enthalpies (BDEs) of 77–92 kcal/mol,[27−29] a range which is

Received: April 22, 2014
Published: July 10, 2014

   dx.doi.org/10.1021/ic500943k | *Inorg. Chem.* 2014, 53, 7622−7634

thermodynamically compatible with the transfer of hydrogen atoms to $Y_zO\bullet$ (the O−H BDE of tyrosine is 86 kcal/mol).[30]

Although synthetic inorganic chemistry has provided numerous examples of multinuclear manganese complexes with bridging hydroxides,[27,29,31−38] mononuclear manganese complexes with terminal hydroxide ligands are comparatively less common. Indeed, to the best of our knowledge, crystal structures have been reported for only eight mononuclear Mn^{III}−OH complexes.[39−46] In these structures, the Mn−OH distances range from 1.81 Å to 1.86 Å, with the longer distances observed for complexes where the hydroxo ligand is involved in hydrogen bonding.[40,41] In fact, intermolecular or intramolecular hydrogen bonding is observed in many of the solid-state structures.[39−41,46] In several structurally characterized complexes, the hydroxo ligand is sterically shielded by the supporting ligand,[40,44,45] which presumably disfavors formation of hydroxo-bridged, multinuclear complexes. Notably, several mononuclear Mn^{III}−OH complexes were generated by treatment of the corresponding manganese(II) species with dioxygen.[44−47]

While the number of known synthetic Mn^{III}−OH complexes is small, the number of such species that participate in PCET reactions is even smaller. To the best of our knowledge, the only reported example of C−H bond oxidation by a synthetic Mn^{III}−OH adduct is found in the $[Mn^{III}(OH)(PY5)]^{2+}$ complex of Stack and co-workers (Figure 1, left; PY5 = 2,6-bis(bis(2-pyridyl)methoxymethane)pyridine).[39] This complex is capable of oxidizing hydrocarbon substrates with C−H BDEs ranging from ∼75−88 kcal/mol by a CPET mechanism.

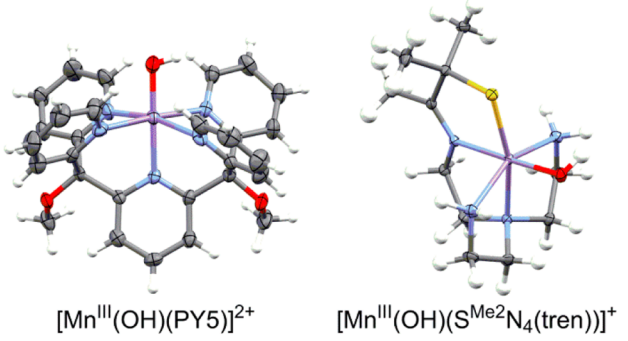

Figure 1. X-ray diffraction (XRD) structures of the cationic fragments of $[Mn^{III}(OH)(PY5)](ClO_4)_2$[39] (left) and $[Mn^{III}(OH)(S^{Me2}N_4(tren))](PF_6)\cdot H_2O$[46] (right).

Kovacs and co-workers recently reported a Mn^{III}−OH adduct supported by the monoanionic N_4S ligand $S^{Me2}N_4(tren)$ (Figure 1, right), which is capable of O−H bond oxidation of TEMPOH (TEMPOH = 2,2′-6,6′-tetramethylpiperidine-1-ol)).[46] TEMPOH is an ideal substrate for investigating CPET reactivity, because it has a relatively weak O−H bond (in MeCN, BDE = 70.6 kcal/mol; bond dissociation free energy (BDFE) = 66.5 kcal/mol), and, when occurring separately, both its deprotonation and one-electron oxidation are quite unfavorable thermodynamically (pK_a = 41 and $E°$ = 0.71 V vs $FeCp_2^+/FeCp_2$ in MeCN).[48] Thus, TEMPOH oxidation proceeds by a CPET mechanism, unless it is reacting with an exceptionally strong base or one-electron oxidant. The $[Mn^{III}(OH)(S^{Me2}N_4(tren))_2]^+$ complex quantitatively converted TEMPOH to TEMPO, with a second-order rate constant of 2.1 × 10^3 M^{-1} s^{-1} at 25 °C in MeCN.[46] A TEMPOH/TEMPOD KIE of 3.1 was observed, consistent with the expected CPET mechanism. Interestingly, the $[Mn^{III}(OH)(S^{Me2}N_4(tren))]^+$ complex was formed by hydrolysis of the oxo-bridged species $[Mn^{III}_2(\mu\text{-}O)(S^{Me2}N_4(tren))_2]^{2+}$, which itself was generated through O_2 oxidation of the $[Mn^{II}(S^{Me2}N_4(tren))]^+$ precursor complex.[46] Because the reaction of $[Mn^{III}(OH)(S^{Me2}N_4(tren))]^+$ with TEMPOH regenerates $[Mn^{II}(S^{Me2}N_4(tren))]^+$, this Mn system served as an aerobic oxidation catalyst for TEMPOH, with at least 10 turnovers.[46]

In this present work, we report a new Mn^{III}−OH complex, $[Mn^{III}(OH)(dpaq)]^+$, featuring the previously reported monoanionic N_5 ligand dpaq[49−51] (dpaq = 2-[bis(pyridin-2-ylmethyl)]amino-*N*-quinolin-8-yl-acetamidate). This complex is generated by treatment of the corresponding $[Mn^{II}(dpaq)](OTf)_2$ species with dioxygen in MeCN at room temperature and is remarkably stable, decaying by only 10% when stored in MeCN solution at 25 °C for 1 week. $[Mn^{III}(OH)(dpaq)]^+$ is capable of oxidizing TEMPOH by a CPET mechanism. The oxidation of the hydrocarbon xanthene (BDFE = 73.3 kcal/mol in dimethylsulfoxide) is also observed. In addition, this complex can oxidize phenolic substrates with BDFEs (in MeCN) up to 78.5 kcal/mol. Intriguingly, saturation behavior is observed in phenol oxidation by $[Mn^{III}(OH)(dpaq)]^+$ but not in TEMPOH oxidation. A plausible explanation for these unusual results and the relevance of this work within the broader context of transition-metal-mediated CPET reactions is discussed.

MATERIALS AND METHODS

All procedures, including the generation of $[Mn^{II}(dpaq)](OTf)$ and organic substrates, as well as kinetic experiments, were carried out under an argon atmosphere, unless otherwise stated. Acetonitrile, methanol, and ether were degassed and dried using a Pure Solv Micro (2010) solvent purification system. These solvents were degassed in airtight solvent reservoirs (4 L), by bubbling Ar gas through the solvent for 20 min at room temperature. Acetonitrile and ether were dried using airtight alumina columns, and methanol was dried using a drierite column. Anhydrous dichloromethane was purchased from Acros Organics (99.9% purity), and was degassed by four freeze−pump−thaw cycles using Schlenk techniques. All solvents were taken into an argon filled glovebox immediately after dispensing from the solvent purification system or following the freeze−pump−thaw cycles, and were stored in tightly sealed Schlenk glassware. The purity of O_2 gas used was >99% and was further purified by passage through a column containing drierite and 5 Å molecular sieves prior to use. TEMPOH, TEMPOD, and 2,4,6-tri-*t*-butylphenol-*d* ($^{4\text{-}t\text{-butyl}}$ArOD) were prepared according to literature procedures,[52,53] and >99% deuteration of TEMPOD and $^{4\text{-}t\text{-butyl}}$ArOD was confirmed by ^{1}H NMR experiments.

Preparation of $[Mn^{II}(dpaq)](OTf)$. $[Mn^{II}(dpaq)](OTf)$ was generated in high yield (>90%) by reacting the H-dpaq ligand with $Mn^{II}(OTf)_2$ in the presence of NaO^tBu in MeOH under an inert atmosphere. The $Mn^{II}(OTf)_2$ salt was generated using a previously reported method.[54] The detailed metallation procedure is as follows. To a stirred solution of 100 mg (0.26 mmol) of H-dpaq in 2 mL of MeOH was added 92 mg (0.26 mmol) of $Mn^{II}(OTf)_2$ in 2 mL of MeOH, followed by 25 mg (0.26 mmol) of NaO^tBu in 2 mL of MeOH under an inert atmosphere. The orange-colored resultant solution was stirred overnight and then the solvent was evaporated to dryness under vacuum. The solid product was recrystallized using MeOH/Et_2O to yield orange-colored crystals of $[Mn^{II}(dpaq)](OTf)$. Crystals for X-ray diffraction (XRD) analysis were obtained by subsequent recrystallization of the final solid product in the MeOH/Et_2O solvent system. $[Mn^{II}(dpaq)](OTf)$ was further characterized by ESI-MS and effective magnetic moment analysis by the ^{1}H NMR method of Evans[55] in CD_3CN at 298 K. ESI-MS (Figure S1 in the Supporting Information): $\{[Mn^{II}(dpaq)]^+\}$ m/z = 437.0994 (calc. 437.1048). The effective magnetic moment (μ_{eff}) was found to be

dx.doi.org/10.1021/ic500943k | Inorg. Chem. 2014, 53, 7622−7634

6.26μ_B, which compares well with the expected value (μ_{eff} = 5.92μ_B) for mononuclear high-spin Mn^{II} centers. Elemental analysis $[Mn^{II}(dpaq)](OTf)$: $C_{24}H_{20}F_3MnN_5O_4S$ calc. (%): C 49.15, H 3.44, N 11.94; found (%): C 48.96, H 3.51, N 11.79.

X-ray Diffraction Data Collection and Analysis for $[Mn^{II}(dpaq)](OTf)$. All XRD experiments were performed on a Bruker Proteum Single Crystal Diffraction System equipped with Helios multilayer optics, an APEX II CCD detector, and a Bruker MicroSTAR microfocus rotating-anode X-ray source operating at 45 kV and 60 mA. The Bruker software package SHELXTL was used to solve the structures using "direct methods" techniques. All stages of weighted full-matrix least-squares refinement were conducted using F_0^2 data with the SHELXTL Version 2010.3−0 software package.[56]

Yellow single crystals of the triflate salt for the cationic polymer, $[Mn(C_{23}H_{19}N_5O)^+]_n$ are, at 100(2) K, monoclinic, space group Cc-C_s^4 (No. 9)[57] with a = 28.6094(9) Å, b = 9.2197(3) Å, c = 28.5260(9) Å, β = 100.550(1)°, V = 7397.1(4) Å^3, and Z = 4 ($[Mn(C_{23}H_{19}N_5O)]_3[CF_3SO_3]_3$) formula units {$d_{calcd}$ = 1.577 g/cm^3; μ_a(Cu Kα) = 5.729 mm^{-1}}. A full set of unique diffracted intensities [5241 frames with counting times of 2−4 s and an ω- or ϕ-scan width of 0.50°] was measured[58] for a single-domain specimen using monochromated Cu Kα radiation (λ = 1.54178 Å). Lattice constants were determined with the Bruker SAINT software package using peak centers for 9466 reflections. A total of 30828 integrated reflection intensities having 2θ(Cu Kα) < 139.58° were produced using the Bruker program SAINT;[59] 9683 of these reflections were unique and gave R_{int} = 0.037. The data were corrected empirically for variable absorption effects using equivalent reflections; the relative transmission factors ranged from 0.836 to 1.000.

The final structural model incorporated anisotropic thermal parameters for all nonhydrogen atoms and isotropic thermal parameters for all hydrogen atoms. Hydrogen atoms were included in the structural model at idealized positions (sp^2- or sp^3-hybridized geometry and C−H bond lengths of 0.95−0.99 Å) with isotropic thermal parameters fixed at values 1.20 times the equivalent isotropic thermal parameter of the carbon atom to which they are covalently bonded.

A total of 1028 parameters were refined using 2 restraints, 9683 data points, and weights of $w = 1/[\sigma^2(F^2) + (0.0563P)^2 + (12.3197P)]$, where $P = [F_0^2 + 2F_c^2]/3$. Final agreement factors at convergence for $[Mn(C_{23}H_{19}N_5O)^+]_n$ are R_1(unweighted, based on F) = 0.037 for 9583 independent absorption-corrected "observed" reflections having 2θ(Cu Kα) < 139.58° and $I > 2\sigma(I)$; R_1(unweighted, based on F) = 0.037 and wR_2(weighted, based on F^2) = 0.096 for all 9683 independent absorption-corrected reflections having 2θ(Cu Kα) < 139.58°. The largest shift/s.u. was 0.001 in the final refinement cycle. The final difference map had maxima and minima of 1.30 and −0.52 e$^-$/Å^3, respectively.

Preparation of $[Mn^{III}(OH)(dpaq)](OTf)$. $[Mn^{III}(OH)(dpaq)](OTf)$ was formed by reacting a 2.5 mM $[Mn^{II}(dpaq)](OTf)$ solution in MeCN with excess O_2 gas at room temperature. The formation of $[Mn^{III}(OH)(dpaq)](OTf)$ was monitored by electronic absorption spectroscopy, as the Mn^{III} complex has characteristic features at 550 and 780 nm. A representative formation reaction is as follows. A 2.5 mM $[Mn^{II}(dpaq)](OTf)$ solution (2.9 mg in 2 mL of MeCN) was prepared under an inert atmosphere and transferred to a gas-tight cuvette sealed with a pierceable septum. An excess of O_2 gas was then delivered to the solution by means of a syringe, and the formation of $[Mn^{III}(OH)(dpaq)](OTf)$ was monitored by electronic absorption spectroscopy. The formation was complete in ∼40 min and the resulting dark gold solution was evaporated to dryness under reduced pressure. The solid residue was then recrystallized using MeCN/Et_2O (3.1 mg/98% yield). Synthesis of $[Mn^{III}(OH)(dpaq)](OTf)$ on a larger scale was undertaken to obtain suitable material for X-ray crystallographic and kinetic experiments. In this procedure, O_2 gas was passed through an acetonitrile solution (20 mg in 5 mL) of $[Mn^{II}(dpaq)](OTf)$, and the completion of the formation of $[Mn^{III}(OH)(dpaq)](OTf)$ was confirmed by ESI-MS and electronic absorption spectroscopy. The resulting solution was evaporated to dryness under reduced pressure, and the solid residue was recrystallized using MeCN/Et_2O. Dark gold $[Mn^{III}(OH)(dpaq)](OTf)$ crystals of X-ray crystallographic quality were obtained by repetitive recrystallization, and were further characterized by ESI-MS and effective magnetic moment (μ_{eff}) analysis by the ^{1}H NMR method of Evans in CD_3CN at 298 K. ESI-MS (Figure S1 in the Supporting Information): $\{[Mn^{III}(OH)(dpaq)]^+\}$ m/z = 454.1056 (calc. 454.1076). μ_{eff} found was 4.88 μ_B (at 298 K for 5 mM solution in CD_3CN) which compares well with the calculated value of 4.89 μ_B for a monomeric high-spin d^4 system. This value is also in close comparison with previously reported solution magnetic susceptibility values for mononuclear hydroxomanganese(III) complexes (μ_{eff} = 4.7 μ_B for $[Mn^{III}(OH)(PY5)]^+$ and μ_{eff} = 4.89 μ_B for $[Mn^{III}(OH)(S^{Me2}N_4(tren))_2]^+$).[39,46] Cyclic voltammetric studies of $[Mn^{III}(OH)(dpaq)](OTf)$ were conducted under an argon atmosphere in acetonitrile (12.89 mg in 10 mL) at 298 K. A 0.1 M acetonitrile solution of $Bu_4N(PF_6)$ was used as the supporting electrolyte, and a glassy carbon working electrode, a platinum auxiliary electrode, and a AgCl/Ag reference electrode were used. Elemental analysis $[Mn^{III}(OH)(dpaq)](OTf)$: $C_{24}H_{21}F_3MnN_5O_5S$ calc. (%): C 47.77, H 3.51, N 11.61; found (%): C 47.26, H 3.65, N 11.62.

X-ray Diffraction Data Collection and Analysis for $[Mn^{III}(OH)(dpaq)](OTf)$. Dark gold single crystals of the CH_3CN solvated salt, $[Mn(OH)(C_{23}H_{20}N_5O)][CF_3SO_3]$, are, at 100(2) K, monoclinic, space group $P2_1/n$ (an alternate setting of $P2_1/c$−C_{2h}^5 (No. 14))[57] with a = 9.2406(3) Å, b = 24.7263(8) Å, c = 12.2658(4) Å, β = 97.257(1)°, V = 2780.1(2) Å^3, and Z = 4 formula units {d_{calcd} = 1.540 g/cm^3; μ_a(Cu Kα) = 5.176 mm^{-1}}. A full set of unique diffracted intensities [5226 frames with counting times of 1 to 3 s and an ω- or ϕ-scan width of 0.50°] was measured[58] for a single-domain specimen using monochromated Cu Kα radiation (λ = 1.54178 Å). Lattice constants were determined with the Bruker SAINT software package using peak centers for 9628 reflections. A total of 25663 integrated reflection intensities having 2θ(Cu Kα) < 139.63° were produced using the Bruker program SAINT;[59] 5017 of these were unique and gave R_{int} = 0.039. The data were corrected empirically for variable absorption effects using equivalent reflections; the relative transmission factors ranged from 0.689 to 1.000.

The triflate anion is 85/15 disordered between two closely spaced sites in the asymmetric unit. This disorder produces a slightly elongated anisotropic thermal ellipsoid for oxygen O(11) in the major-occupancy triflate anion. The bond lengths and angles for the minor-occupancy (15%) triflate were restrained to have values similar to those of the major-occupancy anion. The final structural model incorporated anisotropic thermal parameters for all nonhydrogen atoms of the metal cation, major-occupancy triflate anion, and the CH_3CN solvent molecule. The nonhydrogen atoms for the minor-occupancy triflate anion were incorporated with isotropic thermal parameters. The hydrogen atoms were located from a difference Fourier and included in the structural model as individual isotropic atoms. The positional and thermal parameters for hydrogen atoms and the minor-occupancy triflate were allowed to vary in least-squares refinement cycles.

A total of 509 parameters were refined using 19 restraints, 5017 data points, and weights of $w = 1/[\sigma^2(F^2) + (0.0291P)^2 + (2.4398P)]$, where $P = [F_0^2 + 2F_c^2]/3$. Final agreement factors at convergence are R_1(unweighted, based on F) = 0.031 for 4941 independent absorption-corrected "observed" reflections having 2θ(Cu Kα) < 139.63° and $I > 2\sigma(I)$; R_1(unweighted, based on F) = 0.031 and wR_2(weighted, based on F^2) = 0.079 for all 5017 independent absorption-corrected reflections having 2θ(Cu Kα) < 139.63°. The largest shift/s.u. was 0.001 in the final refinement cycle. The final difference map had maxima and minima of 0.49 and −0.58 e$^-$/Å^3, respectively.

Kinetic Studies of $[Mn^{III}(OH)(dpaq)](OTf)$ with Substituted Phenols. For each kinetic experiment, a 1.25 mM $[Mn^{III}(OH)(dpaq)]^+$ (1.6 mg, 2.5 × 10^{-3} mmol) solution was prepared in acetonitrile (2 mL) within an argon-filled glovebox, transferred to a gas-tight cuvette sealed with a pierceable septum. A solution of the phenolic substrate was prepared in dichloromethane (300 μL) and sealed in a 4 mL glass vial with a pierceable septum. Then, the cuvette containing the $[Mn^{III}(OH)(dpaq)]^+$ solution was inserted into a

dx.doi.org/10.1021/ic500943k | Inorg. Chem. 2014, 53, 7622−7634

temperature-controlled cryostat (Unisoku), held at 50 °C, coupled to an Agilent 8453 UV/Visible spectrophotometer. Upon achieving thermal equilibrium (10 min), data collection was started, and 100 μL of the substrate solution was injected into the cuvette using a gas-tight syringe. Data collection times ranged from 3000 s to 6000 s. An aliquot of the final reaction mixture was analyzed by perpendicular-mode X-band electron paramagnetic resonance (EPR) spectroscopy at 5 K and revealed signals consistent with $[Mn^{II}(dpaq)]^+$ and a phenoxyl radical (see Figure S2 in the Supporting Information). The rates of the reactions were calculated by applying initial rate approximation (initial 20% of the disappearance of $[Mn^{III}(OH)(dpaq)]^+$ was monitored at 800 nm) in order to prevent any interference by side reactions at longer time scales. These initial rates (in absorbance units/time) were converted into s^{-1} units by using the absorption coefficient (ε_{800} = 130 M^{-1} cm^{-1}) and initial concentration (1.25 mM) of $[Mn^{III}(OH)(dpaq)]^+$. The kinetic data for reactions with greater than 10 equiv 2,4,6-tri-*t*-butylphenol were collected to five half-lives and fit directly to obtain a pseudo-first-order rate constant. In these cases, the directly obtained pseudo-first-order rate constants were identical, within error, to those obtained using the initial rate method.

Kinetic Studies of $[Mn^{III}(OH)(dpaq)](OTf)$ with TEMPOH. Similar to the kinetic experiments with phenols, a 1.25 mM $[Mn^{III}(OH)(dpaq)]^+$ (1.6 mg, 2.5 × 10^{-3} mmol) solution was prepared in acetonitrile (2 mL) within an argon-filled glovebox, and was sealed in a gastight cuvette with a pierceable septum. The TEMPOH solution was prepared in acetonitrile (100 μL) and sealed in a 300 μL glass vial with a pierceable septum. Data collection was started, and the TEMPOH solution was added into the $[Mn^{III}(OH)(dpaq)]^+$ solution using a gas-tight syringe (at 25 °C). Data collection times ranged from 200 s to 4000 s. A final reaction mixture analyzed by perpendicular-mode X-band EPR spectroscopy at 5 K revealed characteristic features consistent with the presence of the TEMPO radical (see Figure S2 in the Supporting Information). Kinetic experiments at variable temperatures (−15 °C to 45 °C (258−318 K)) were performed following the same procedure as described, allowing the cuvette to achieve thermal equilibrium (10 min) in the cryostat, prior to the addition of the substrate.

Kinetic Studies of $[Mn^{III}(OH)(dpaq)](OTf)$ with Xanthene. For each experiment, a 1.25 mM $[Mn^{III}(OH)(dpaq)]^+$ (1.6 mg, 2.5 × 10^{-3} mmol) solution was prepared in acetonitrile (2 mL) within an argon-filled glovebox. This solution was transferred to a gas-tight cuvette and sealed with a pierceable septum. The xanthene solution was prepared in dichloromethane (200 μL) and sealed in a 4-mL glass vial with a pierceable septum. Then, the cuvette containing the $[Mn^{III}(OH)(dpaq)]^+$ solution was inserted into a temperature-controlled cryostat held at 50 °C. Upon achieving thermal equilibrium, data collection was started, and 100 μL of the xanthene solution was injected into the cuvette using a gas-tight syringe. Data collection was carried out up to ∼900 min. The rates of the reactions were calculated by applying initial rate approximation in order to exclude any interference by secondary reactions.

Catalytic Oxidation of TEMPOH with $[Mn^{III}(OH)(dpaq)](OTf)$. For each experiment, $[Mn^{II}(dpaq)]^+$ (initial concentration = 0.031 mM) and TEMPOH (initial concentration = 125 mM) were measured into a 20-mL glass vial within an argon-filled glovebox and dissolved in acetonitrile (2 mL). This solution was sealed in a gas-tight cuvette with a pierceable septum, and the electronic absorption spectrum was collected under ambient conditions (∼25 °C). Then, an excess of dry dioxygen gas was bubbled through the solution, while electronic absorption spectra were collected every ∼15 min. The solvent level of the reaction mixture was closely monitored confirming a negligible solvent evaporation during oxygenation.

RESULTS AND ANALYSIS

Structural Properties of $[Mn^{II}(dpaq)](OTf)$. The XRD structure of $[Mn^{II}(dpaq)](OTf)$ shows three $[Mn^{II}(dpaq)](OTf)$ molecules in the smallest asymmetric unit. Although these three molecules do show slight differences in bond lengths and angles, each consists of a Mn^{II} center in a highly distorted octahedral geometry (Figure 2), with two pyridine ligands (N4, N5), the quinoline ligand (N1) and the tertiary amine (N3) in the equatorial plane, and the amide nitrogen (N2) occupying an axial position. The other axial site is occupied by the amide oxygen atom (O1) of a second $[Mn^{II}(dpaq)](OTf)$ molecule, forming an overall polymeric structure. Table 1 summarizes the structural properties for one of the $[Mn^{II}(dpaq)]^+$ cations in the asymmetric unit (cation B); corresponding metric parameters for the other cations can be found in Table S3 in the Supporting Information. For the three cations, the angle between the axial ligands (O1−Mn−N2) is ∼165°−170° and the angles between the equatorial ligands vary from ∼75° to ∼105°, indicating large deviations from idealized octahedral geometry. Three triflate ions are also present in the crystal structure but do not interact with the Mn^{II} centers (Mn−O distances of ∼6.4 Å). All Mn^{II}−ligand distances are in the range of 2.1−2.3 Å, which is typical for a high-spin Mn^{II} center. Notably, the C10−O1 distance of the amide ranges from 1.265(4) Å to 1.271(4) Å, which is typical of

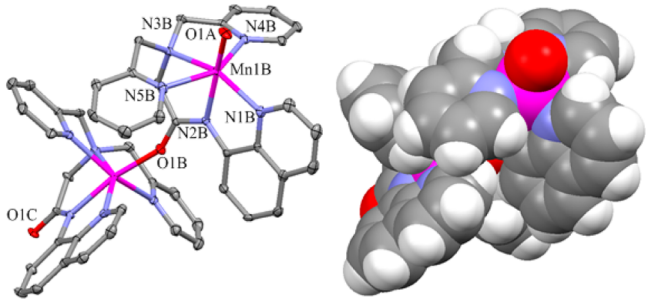

Figure 2. ORTEP (left) and space filling (right) diagrams showing two cations (B and C) in the asymmetric unit of the X-ray structure of $[Mn^{II}(dpaq)](OTf)$. ORTEP diagram shows 50% probability thermal ellipsoids. Hydrogen atoms and noncoordinating triflate counteranions have been removed for clarity. Significant interatomic distances and angles are listed in Table 1 and in Table S3 in the Supporting Information.

Table 1. Selected Bond Lengths and Angles for $[Mn^{II}(dpaq)](OTf)$ and $[Mn^{III}(OH)(dpaq)](OTf)$

Bond Length		Bond Angle	
atom pair	value	angle	value
	$[Mn^{II}(dpaq)]^+$ (B)[a]		
Mn−O1A	2.079(2) Å	O1A−Mn−N2B	164.88(10)°
Mn−N2B	2.191(3) Å	N4B−Mn−N5B	147.89(11)°
Mn−N1B	2.214(3) Å	N1B−Mn−N3B	151.40(10)°
Mn−N3B	2.314(3) Å	N4B−Mn−N2B	94.97(10)°
Mn−N4B	2.244(3) Å	N1B−Mn−N2B	74.46(10)°
Mn−N5B	2.286(3) Å	N3B−Mn−N2B	77.52(10)°
	$[Mn^{III}(OH)(dpaq)](OTf)$		
Mn−O2	1.806(13) Å	O2−Mn−N2	177.94(6)°
Mn−N2	1.975(14) Å	N4−Mn−N5	152.53(5)°
Mn−N1	2.072(14) Å	N1−Mn−N3	161.83(6)°
Mn−N3	2.173(14) Å	N4−Mn−N2	85.22(5)°
Mn−N4	2.260(14) Å	N1−Mn−N2	79.77(6)°
Mn−N5	2.216(15) Å	N3−Mn−N2	82.51(6)°

[a]Bond lengths and angles for one of the three $[Mn^{II}(dpaq)]^+$ cations in the asymmetric unit. Corresponding metric parameters for the other two cations are given in Table S3 in the Supporting Information.

dx.doi.org/10.1021/ic500943k | Inorg. Chem. 2014, 53, 7622−7634

a C=O double bond. Thus, the Mn−O1 interaction is likely weak, and presumably the polymeric structure observed in the crystal structure reverts to separate monomeric entities in solution. Overall, the structure of $[Mn^{II}(dpaq)](OTf)$ compares well with that of a recently reported $[Mn(dpaq)(NO)](ClO_4)$ complex, although the latter species showed shorter manganese-ligand bond lengths.[49] The shorter bond lengths in $[Mn(dpaq)(NO)](ClO_4)$ are expected given the formulation of that complex as a low-spin Mn^{II} center antiferromagnetically coupled to an NO radical.

Formation of $[Mn^{III}(OH)(dpaq)](OTf)$. The absorption spectrum of $[Mn^{II}(dpaq)](OTf)$ in acetonitrile shows a very weak band at 510 nm (ε = 24 M^{-1} cm^{-1}). When treated with excess O_2 gas at 25 °C, the light orange-colored $[Mn^{II}(dpaq)](OTf)$ solution rapidly changed its color to dark gold, as new absorption features grew in at 550 nm (ε = 320 M^{-1} cm^{-1}) and 780 nm (ε = 130 M^{-1} cm^{-1}) (Figure 3; the extinction

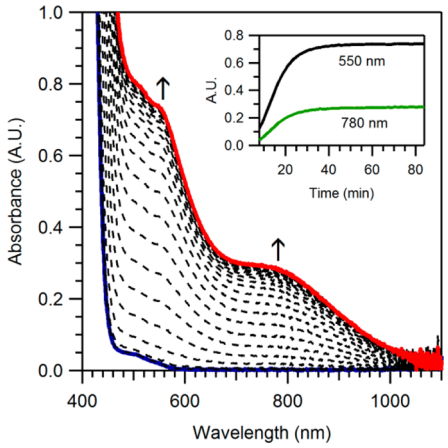

Figure 3. Electronic absorption spectra of 2.5 mM $[Mn^{II}(dpaq)]^+$ (solid blue trace) upon the addition of excess O_2 at 25 °C in MeCN under argon. Inset: Time evolution of absorption signals at 550 and 780 nm.

coefficients were obtained using recrystallized $[Mn^{III}(OH)(dpaq)](OTf)$). Formation of these new electronic absorption features is consistent with the oxidation of Mn^{II} upon reacting with O_2. Electronic absorption spectral signatures for other hydroxomanganese(III) species vary in terms of their energies,[43,45,46] although the closely related $[Mn^{III}(OH)(PaPy_2Q)]ClO_4$ complex (where $PaPy_2Q$ is the amide-containing N_5 ligand *N*,*N*-bis(2-pyridylmethyl)-amine-*N*-ethyl-2-quinoline-2-carboxamide) has spectral features with striking similarities to those of $[Mn^{III}(OH)(dpaq)](OTf)$.[42] The prominent absorption signatures for $[Mn^{III}(OH)(PaPy_2Q)]ClO_4$ in acetonitrile are centered at 485 nm (ε = 280 M^{-1} cm^{-1}) and 740 nm (ε = 120 M^{-1} cm^{-1}). These similarities between the electronic absorption features are anticipated given the closely related primary coordination spheres of $[Mn^{III}(OH)(PaPy_2Q)]ClO_4$ and $[Mn^{III}(OH)(dpaq)](OTf)$ (vide infra). The final product $[Mn^{III}(OH)(dpaq)](OTf)$ was isolated in an essentially quantitative yield of greater than 98%. The half-life ($t_{1/2}$) of $[Mn^{III}(OH)(dpaq)](OTf)$ was estimated by monitoring the electronic absorption spectrum of a 1.25 mM acetonitrile solution at 25 °C. The concentration of $[Mn^{III}(OH)(dpaq)]^+$ decreased by ∼10% after 6 days. Assuming a constant decay rate, the half-life of $[Mn^{III}(OH)(dpaq)](OTf)$ under these conditions is estimated to be 26 days.

Properties of $[Mn^{III}(OH)(dpaq)](OTf)$. The X-ray structure of $[Mn^{III}(OH)(dpaq)](OTf)$ contains a six-coordinate Mn^{III} center with a distorted octahedral geometry (Figure 4).

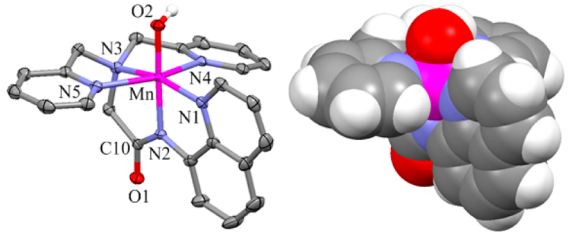

Figure 4. ORTEP (left) and space filling (right) diagrams of $[Mn^{III}(OH)(dpaq)](OTf)$. ORTEP diagram shows 50% probability thermal ellipsoids. Hydrogen atoms and noncoordinating triflate counteranion have been removed for clarity. Significant interatomic distances and angles are listed in Table 1.

Coordination of the dpaq ligand is the same as in $[Mn^{II}(dpaq)](OTf)$, with the exception that all Mn−N bonds, other than Mn−N4, are shorter in $[Mn^{III}(OH)(dpaq)](OTf)$ by 0.062−0.202 Å (Table 1). The hydroxide group in $[Mn^{III}(OH)(dpaq)](OTf)$ is trans to the amide nitrogen, with a Mn−O2 distance of 1.806(13) Å. Inspection of the extended structure of $[Mn^{III}(OH)(dpaq)]^+$ reveals that the hydrogen atom of the hydroxo ligand is involved in a hydrogen-bonding interaction with the amide oxygen of an adjacent $[Mn^{III}(OH)(dpaq)]^+$ molecule (O···O and H···O separations of 2.7308(18) and 1.95(3) Å, respectively). A free triflate ion and an acetonitrile molecule are observed within the asymmetric unit, but these are not associated with the metal center (Mn−O and Mn−N distances of ∼6.2 and ∼4.8 Å for triflate oxygen and acetonitrile nitrogen, respectively).

There have been several X-ray structures of mononuclear Mn^{III}−OH complexes, and these have revealed Mn−O(H) distances within the range of 1.81−1.86 Å.[39−46] The longest distance of 1.86 Å is unusual, and represents hydrogen-bonding interactions with an ordered cluster of water molecules in the solid-state.[41] The $[Mn^{III}(OH)(dpaq)]^+$ complex has a Mn−O(H) distance of 1.806(13) Å, which is at the lower end of the range of previously reported distances for this class of compounds. The O2−Mn−N2 axis, which includes the hydroxide oxygen and amide nitrogen ligands, represents the compressed pseudo-Jahn−Teller axis. The observation of an intermolecular hydrogen-bond involving the hydroxo ligand in $[Mn^{III}(OH)(dpaq)]^+$ is not unusual. Four of the eight known X-ray structures of Mn^{III}−OH adducts show second-sphere hydrogen-bonding interactions in the solid-state structures.[39−41,46]

Cyclic voltammetric analysis of $[Mn^{III}(OH)(dpaq)](OTf)$ in acetonitrile revealed a partially reversible wave with an $E_{1/2}$ of −0.60 V vs Fc^+/Fc at a scan rate of 100 mV s^{-1} (ΔE_p = 120 mV; see Figure S3 in the Supporting Information), which we attribute to the Mn^{III}/Mn^{II} couple. This potential value is comparable to that reported for the reduction of $[Mn^{III}(OH)(S^{Me2}N_4(tren))_2]^+$ ($E_{p,c}$ = −0.6 V vs Fc^+/Fc in MeCN).[46] Previous studies have also described Mn^{III}/Mn^{II} reduction potentials for several other hydroxomanganese(III) complexes. Stack and co-workers reported that $[Mn^{III}(OH)(PY5)]^{2+}$ (Figure 1, left) exhibited a quasi-reversible reduction wave at $E_{1/2}$ = +0.17 V vs Fc^+/Fc (reported as +0.81 V vs SHE; ΔE_p =

dx.doi.org/10.1021/ic500943k | Inorg. Chem. 2014, 53, 7622−7634

150 mV), which was attributed to the Mn^{III}/Mn^{II} couple.[39] The higher reduction potential for this dicationic complex compared to that of $[Mn^{III}(OH)(dpaq)]^+$ is anticipated given the difference in overall charge of the two complexes. Furthermore, a monoanionic hydroxomanganese(III) species supported by a trianionic ligand has a Mn^{III}/Mn^{II} couple at −1.51 V vs Fc^+/Fc (ΔE_p = 380 mV).[60] An outlier from this trend is $[Mn^{III}(OH)(OAc)(Me_2EBC)]^+$ (Me_2EBC = 4,11-dimethyl-1,4,8,11-tetraazabicyclo[6.6.2]hexadecane), for which $E_{1/2}$ = −1.33 V vs Fc^+/Fc (reported as −0.689 V vs SHE; ΔE_p = 132 mV). This deviation is presumably due to the preferential stabilization of Mn^{III} within the cavity of the macrocyclic supporting ligand.[45]

Reactivity of $[Mn^{III}(OH)(dpaq)]^+$ with TEMPOH. The isolation of $[Mn^{III}(OH)(dpaq)]^+$ allowed us to investigate the ability of this species to effect PCET reactions. Treatment of $[Mn^{III}(OH)(dpaq)]^+$ with 100 equiv TEMPOH under an argon atmosphere in MeCN at 25 °C lead to the rapid disappearance of the electronic absorption bands of $[Mn^{III}(OH)(dpaq)]^+$ (Figure 5). The final electronic absorption spectrum appears essentially identical to that of $[Mn^{II}(dpaq)]^+$ in MeCN, showing a very weak band at 510 nm. Using the intensity of this band, and the extinction coefficient for $[Mn^{II}(dpaq)]^+$ (vide supra), the Mn^{II} complex forms in 99% yield. The perpendicular-mode X-band EPR spectrum of the final reaction mixture at 5 K shows characteristic EPR features of the TEMPO radical centered at g = 2.04 (Figure S2A in the Supporting Information).[61] Together, these data demonstrate that TEMPOH reacts with $[Mn^{III}(OH)(dpaq)]^+$ to generate TEMPO and $[Mn^{II}(OH_2)(dpaq)]$ quantitatively; i.e., the PCET reaction goes to completion under these conditions.

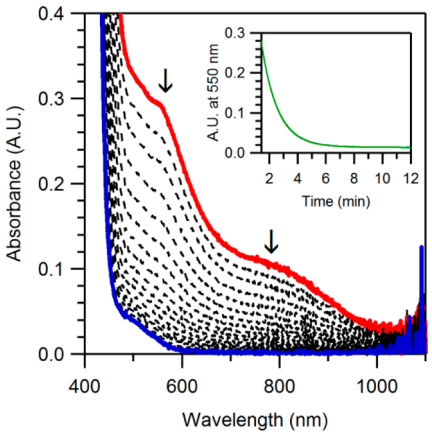

Figure 5. Electronic absorption spectra of 1.25 mM $[Mn^{III}(OH)(dpaq)]^+$ upon the addition of 100 equiv TEMPOH at 25 °C in MeCN under argon. Inset shows the decay of the 550-nm absorption signal.

Kinetic parameters associated with this process were determined through a series of reactions between $[Mn^{III}(OH)(dpaq)]^+$ and 10−250 equiv TEMPOH (pseudo-first-order conditions). In all cases, the decay of $[Mn^{III}(OH)(dpaq)]^+$ followed pseudo-first-order behavior to at least 5 half-lives (Figure 5, inset). The pseudo-first-order rate constants increase linearly as a function of TEMPOH concentration (Figure 6), giving a second-order rate constant of $1.3(1) \times 10^{-1}$ M^{-1} s^{-1} at 25 °C. Using deuterated TEMPOD, a kinetic isotope effect (KIE) of 1.8 was observed (Figure 6). The KIE value, although small, suggests that cleavage of the TEMPO−H/D bond occurs

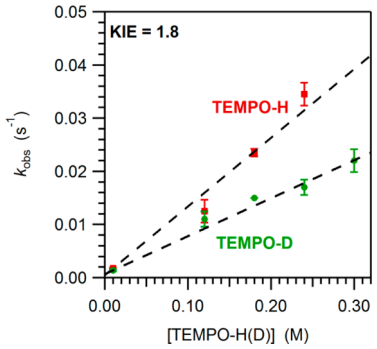

Figure 6. Pseudo-first-order rate constants, k_{obs} (s^{-1}) versus TEMPOH and TEMPOD concentration for a 1.25 mM solution of $[Mn^{III}(OH)(dpaq)]^+$. The second-order rate constant, k_2 (M^{-1} s^{-1}), was calculated from the linear correlation of the observed rate constant and substrate concentration.

in the rate-determining step. Similar KIE values of less than 2.0 have been observed for O−H bond oxidation by other transition-metal species in cases where rate-determining O−H/D bond cleavage has been proposed.[62] Given the exceptionally high pK_a of TEMPOH in MeCN (41),[48] the KIE is supportive of the expected CPET mechanism for this reaction. Moreover, the relatively low reduction potential of $[Mn^{III}(OH)(dpaq)]^+$ rules out a rapid electron transfer process. An Eyring analysis of the reaction of $[Mn^{III}(OH)(dpaq)]^+$ with TEMPOH from −15 °C to 45 °C (258−318 K), afforded activation parameters $\Delta H^‡$ and $\Delta S^‡$ of 9.9(9) kcal/mol and −35(3) cal/(mol K), respectively (Figure 7). Thus, at 25 °C, the entropic contribution to the free energy of activation ($T\Delta S^‡$ = −10 kcal/mol) is equal to the enthalpic contribution.

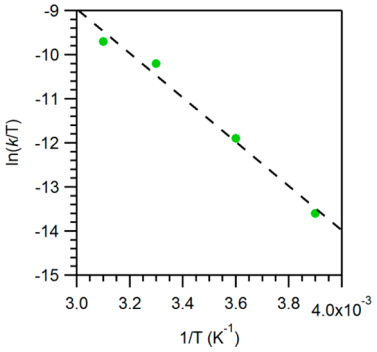

Figure 7. Eyring plot showing $\ln(k/T)$ versus $1/T$ (K^{-1}) for the reaction of 1.25 mM $[Mn^{III}(OH)(dpaq)]^+$ with TEMPOH from −15 °C to 45 °C (258−318 K).

Reactivity of $[Mn^{III}(OH)(dpaq)]^+$ with Xanthene. The addition of 250 equiv of xanthene to a 1.25 mM solution of $[Mn^{III}(OH)(dpaq)]^+$ at 50 °C led to the slow decay of the electronic absorption signals of the Mn^{III}−OH complex (see Figure S4 in the Supporting Information). Over the course of 15 h, after the addition of xanthene, 50% of $[Mn^{III}(OH)(dpaq)]^+$ was observed to disappear. Importantly, $[Mn^{III}(OH)(dpaq)]^+$ itself shows essentially no self-decay in the absence of xanthene in this time period. A pseudo-first-order rate constant of 8×10^{-4} s^{-1} was determined for the reaction of $[Mn^{III}(OH)(dpaq)]^+$ with xanthene using the method of initial rates.

dx.doi.org/10.1021/ic500943k | Inorg. Chem. 2014, 53, 7622−7634

Reactivity of $[Mn^{III}(OH)(dpaq)]^+$ with Phenols. $[Mn^{III}(OH)(dpaq)]^+$ also reacted with 2,4,6-tri-*t*-butylphenol ($^{4\text{-}t\text{-butyl}}$ArOH), which has an O–H bond nearly 11 kcal/mol stronger than that of TEMPOH (BDFE in MeCN of 77.1 and 66.5 kcal/mol, respectively). Monitoring the reaction of $[Mn^{III}(OH)(dpaq)]^+$ with $^{4\text{-}t\text{-butyl}}$ArOH by electronic absorption spectroscopy showed that the decay of the $[Mn^{III}(OH)(dpaq)]^+$ complex is concomitant with the formation of the corresponding phenoxyl radical, $^{4\text{-}t\text{-butyl}}$ArO• ($\lambda_{max}$ = 628 nm; ε = 400(10) M^{-1} cm^{-1} in MeCN at 25 °C; see Figure 8).[63] The

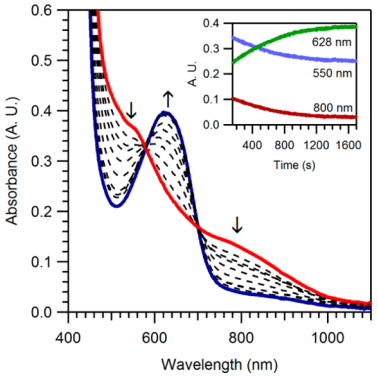

Figure 8. Electronic absorption spectra of 1.25 mM $[Mn^{III}(OH)(dpaq)]^+$ upon the addition of 100 equiv of 2,4,6-tri-*t*-butylphenol ($^{4\text{-}t\text{-butyl}}$ArOH) at 50 °C in MeCN under argon. Inset shows the time evolution of single-wavelength traces at 628, 550, and 800 nm.

phenoxyl radical was formed in 80% yield, relative to the initial $[Mn^{III}(OH)(dpaq)]^+$ concentration. A comparison of perpendicular-mode X-band EPR spectra of $[Mn^{II}(dpaq)]^+$, $[Mn^{III}(OH)(dpaq)]^+$, and the final products of $^{4\text{-}t\text{-butyl}}$ArOH oxidation provides evidence for the formation of $[Mn^{II}(dpaq)]^+$ and the phenoxyl radical following the phenol oxidation reaction (see Figure S2B in the Supporting Information). The 80% yield of the phenoxyl radical was observed regardless of the initial $[Mn^{III}(OH)(dpaq)]^+$:$^{4\text{-}t\text{-butyl}}$ArOH ratio (see Table S4 in the Supporting Information). It is possible that the 80% yield is observed because the radical participates in side reactions that prevent its full accumulation. However, the clean isosbestic behavior observed in the reaction of $[Mn^{III}(OH)(dpaq)]^+$ with $^{4\text{-}t\text{-butyl}}$ArOH (Figure 8) is difficult to reconcile with the disappearance of 20% of the radical product during the timecourse of this reaction. The substoichiometric formation of phenoxyl radical was also noted in the reaction of $[Mn^{III}(OH)(PY5)]^+$ (Figure 1, left) with $^{4\text{-}t\text{-butyl}}$ArOH.[39] For that system, the phenoxyl radical was formed after most of the Mn^{III}–OH complex was consumed, indicating a reaction between the metal complex and the phenoxyl radical. In this present work, the rate of formation of the radical is the same as the rate of disappearance of $[Mn^{III}(OH)(dpaq)]^+$; thus, we assume that no reaction occurs between the Mn^{III} complex and the phenoxyl radical. An alternative explanation for the 80% yield of the phenoxyl radical would be that the equilibrium for the reaction of $[Mn^{III}(OH)(dpaq)]^+$ and $^{4\text{-}t\text{-butyl}}$ArOH to give $[Mn^{II}(OH_2)(dpaq)]^+$ and $^{4\text{-}t\text{-butyl}}$ArO• does not lie very far to the right. This can be discounted by the nearly invariant yield of the phenoxyl radical over a range of initial $[Mn^{III}(OH)(dpaq)]^+$: $^{4\text{-}t\text{-butyl}}$ArOH concentrations (see Table S4 in the Supporting Information).

When $[Mn^{III}(OH)(dpaq)]^+$ was treated with excess $^{4\text{-}t\text{-butyl}}$ArOH (10–125 equiv), the decay of $[Mn^{III}(OH)(dpaq)]^+$ and formation of $^{4\text{-}t\text{-butyl}}$ArO• follow pseudo-first-order kinetics to at least 3 half-lives. Between 10 and 50 equiv of added $^{4\text{-}t\text{-butyl}}$ArOH, the pseudo-first-order rate constants (k_{obs}) show an almost-linear increase, with respect to $^{4\text{-}t\text{-butyl}}$ArOH concentration. However, above 50 equiv $^{4\text{-}t\text{-butyl}}$ArOH, saturation behavior was observed (Figure 9), indicating the formation of

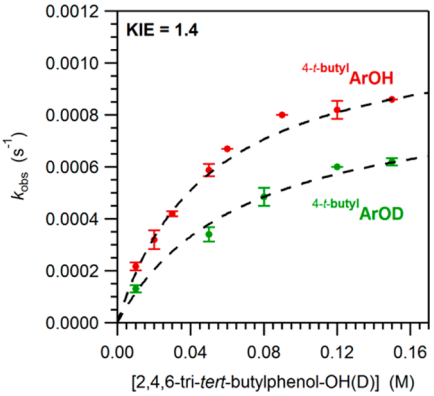

Figure 9. Observed pseudo-first-order rate constants (k_{obs}) as a function of $^{4\text{-}t\text{-butyl}}$ArOH and $^{4\text{-}t\text{-butyl}}$ArOD concentration for $[Mn^{III}(OH)(dpaq)]^+$.

an intermediate prior to the rate-determining step (see Scheme 1). Accordingly, the relationship between k_{obs} and the

Scheme 1. Reaction of $[Mn^{III}(OH)(dpaq)]^+$ with $^{4\text{-}t\text{-butyl}}$ArOH, Where an Initial Equilibrium (K_{eq}) between $[Mn^{III}(OH)(dpaq)]^+$ and $^{4\text{-}t\text{-butyl}}$ArOH Forms an Intermediate, Which Converts to Products via a Rate-Determining Step (k_1)

concentration of $^{4\text{-}t\text{-butyl}}$ArOH was fit using the following equation: $k_{obs} = k_1K_{eq}[^{4\text{-}t\text{-butyl}}\text{ArOH}]/1 + K_{eq}[^{4\text{-}t\text{-butyl}}\text{ArOH}]$, where k_1 is the rate constant (in units of s^{-1}) for the rate-determining step and K_{eq} is the equilibrium constant describing the formation of the intermediate from $[Mn^{III}(OH)(dpaq)]^+$ and $^{4\text{-}t\text{-butyl}}$ArOH (Scheme 1). This analysis afforded a K_{eq} of 20(2) and a k_1 of 1.2(1) × 10^{-3} s^{-1} (Table 2).

A similar analysis was performed for data collected using the deuterated phenol $^{4\text{-}t\text{-butyl}}$ArOD (Figure 9). The K_{eq} value for the reaction using $^{4\text{-}t\text{-butyl}}$ArOD is quite similar to that observed for $^{4\text{-}t\text{-butyl}}$ArOH (Table 2). Considering the standard deviations for the K_{eq} values, these parameters are almost overlapping. The k_1 values for the $^{4\text{-}t\text{-butyl}}$ArOD and $^{4\text{-}t\text{-butyl}}$ArOH substrates afford a KIE of 1.4.

To determine if the observed saturation behavior is a feature of the reaction of $[Mn^{III}(OH)(dpaq)]^+$ with phenolic substrates in general, we explored the reactivity of this complex with a series of phenols, including 4-methoxy-2,6-tri-*t*-butylphenol ($^{4\text{-MeO}}$ArOH), 4-methyl-2,6-tri-*t*-butylphenol ($^{4\text{-Me}}$ArOH), and 2,6-di-*t*-butylphenol ($^{4\text{-H}}$ArOH). This series encompasses a reasonable range of phenol O–H BDFEs (74–78.5 kcal/mol) and pK_a values (23–28), as summarized in Table 2. In reactions with phenols with BDFEs greater than 79 kcal/mol (3,5-di-*t*-butyl-4-hydroxybenzonitrile ($^{4\text{-CN}}$ArOH) and 3,5-di-*t*-butyl-4-

dx.doi.org/10.1021/ic500943k | Inorg. Chem. 2014, 53, 7622–7634

Table 2. Equilibrium and Rate Constants from Kinetic Experiments between $[Mn^{III}(OH)(dpaq)]^+$ and Phenols at 50 °C in MeCN, and Substrate $BDFE_{OH}$, pK_a, and Reduction Potential Values

substrate	K_{eq}	k_1 (s^{-1})	$BDFE_{OH}$[a] (kcal/mol)	pK_a[b]	E[c] (V)
$^{4\text{-MeO}}$ArOH	>700	$1.8(1) \times 10^{-3}$	73.9(1)	28	−0.806
$^{4\text{-Me}}$ArOH	18(1)	$1.5(1) \times 10^{-3}$	76(1)	27	−0.755
$^{4\text{-}t\text{-butyl}}$ArOH	20(2)	$1.2(1) \times 10^{-3}$	77.1(1)	28	−0.645
$^{4\text{-}t\text{-butyl}}$ArOD	15(2)	$8.9(1) \times 10^{-4}$			
$^{4\text{-H}}$ArOH	8(1)	$9.4(1) \times 10^{-4}$	78.5(1)	27	−0.619

[a]Data taken from Warren et al.[48] *or* determined following the work of Waidmann et al.[64] [b]pK_a values in MeCN; see ref 65. [c]Potential for PhO•/PhO^- in DMSO vs $Cp_2Fe^{+/0}$.[48]

hydroxybenzaldehyde ($^{4\text{-CHO}}$ArOH)), only a fraction of $[Mn^{III}(OH)(dpaq)]^+$ was consumed. This implies that the thermodynamic limit for the oxidative capability of this Mn^{III}–OH adduct is ∼80 kcal/mol.

The reactions of $[Mn^{III}(OH)(dpaq)]^+$ with $^{4\text{-MeO}}$ArOH, $^{4\text{-Me}}$ArOH, and $^{4\text{-H}}$ArOH all showed saturation behavior, with the pseudo-first-order rate constants leveling at higher phenol concentration (Figure S5 in the Supporting Information). Equilibrium and rate constants determined from fits to these datasets are collected in Table 2. In the case of $^{4\text{-MeO}}$ArOH, the observed rate was saturated even when using 10 equiv of phenol (Figure S5 in the Supporting Information, top right). Thus, only an estimate of the lower limit for K_{eq} (700) could be obtained for this substrate.

An Evans–Polanyi plot for the oxidation of phenolic substrates with $[Mn^{III}(OH)(dpaq)]^+$ shows a linear dependence of the rate-determining step (k_1) as a function of BDFE of the substrate (Figure 10). This relationship, along with the KIE

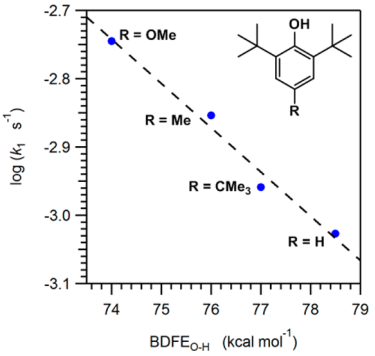

Figure 10. Evans–Polanyi plot of oxidation rate (k_1) of phenolic substrates versus the BDFE of the substrate.

value for the reaction of $[Mn^{III}(OH)(dpaq)]^+$ with $^{4\text{-}t\text{-butyl}}$ArOH, provides strong evidence that the rate-determining step in these reactions is a CPET between the phenol and the Mn^{III}–OH unit. Thus, the pre-equilibrium step shown in Scheme 1 potentially involves the formation of a hydrogen-bonded reactant complex.

To further probe the nature of the intermediate formed in the initial equilibrium reaction between $[Mn^{III}(OH)(dpaq)]^+$ and $^{4\text{-}t\text{-butyl}}$ArOH (Scheme 1), 400 equiv of the phenol were added to a MeCN solution of $[Mn^{III}(OH)(dpaq)]^+$ at 50 °C. Under these conditions, the intermediate species should initially be dominant in solution. Electronic absorption spectra collected 0.5–1.5 s after the addition of $^{4\text{-}t\text{-butyl}}$ArOH show very minor perturbations relative to the spectrum of pure $[Mn^{III}(OH)(dpaq)]^+$ (see Figure S6 in the Supporting Information). Specifically, the observed absorption maxima are not shifted upon $^{4\text{-}t\text{-butyl}}$ArOH addition, and the absorption intensity at 550 nm rises by only 12%. The observed increase in intensity is wavelength dependent and, thus, is potentially due to light scattering, which increases as a function of the fourth power of the light frequency. Under the reasonable assumption that the electronic absorption spectrum of $[Mn^{III}(OH_2)(dpaq)]^{2+}$ should be distinct from that of $[Mn^{III}(OH)(dpaq)]^+$, the similarities between the electronic absorption spectra before and after the addition of the $^{4\text{-}t\text{-butyl}}$ArOH suggest that the intermediate does not result from proton transfer between $^{4\text{-}t\text{-butyl}}$ArOH and $[Mn^{III}(OH)(dpaq)]^+$.

Catalytic Oxidation of TEMPOH with $[Mn^{II}(dpaq)](OTf)$ and O_2. In the presence of a large excess of TEMPOH (4000 equiv), $[Mn^{II}(dpaq)](OTf)$ catalytically converted TEMPOH into TEMPO in continuously oxygenated MeCN solution at 25 °C. The catalytic process was followed over the course of 200 min by electronic absorption spectroscopy, monitoring the characteristic features of TEMPO and $[Mn^{II}(dpaq)](OTf)$ (see Figure S7B in the Supporting Information). The direct oxidation of TEMPOH in the absence of the catalyst was investigated as a control (see Figure S7A in the Supporting Information). Although oxidation of TEMPOH to TEMPO is observed in the control reactions, ∼40% higher conversions are observed in the presence of $[Mn^{II}(dpaq)](OTf)$. Importantly, separate control experiments using catalytic amounts of $Mn^{II}(OTf)_2$ gave results within error of the control experiments lacking any Mn^{II} species. Thus, the increase in turnover numbers is attributed to catalytic activity of the $[Mn^{II}(dpaq)](OTf)$ complex. Correcting for the background oxidation of TEMPOH in the control reactions, a maximum of 1050 turnovers were observed using $[Mn^{II}(dpaq)](OTf)$ as an aerobic oxidation catalyst.

DISCUSSION

Synthetic complexes with mononuclear hydroxomanganese(III) motifs are relatively rare,[39−46,66−69] as the hydroxo ligand is prone to bridge Mn centers.[27,29,31−38] Of the known mononuclear Mn^{III}–OH complexes, only two—$[Mn^{III}(OH)(PY5)]^{2+}$ and $[Mn^{III}(OH)(S^{Me2}N_4(tren))]^+$ (see Figure 1)—have been reported to perform substrate oxidation reactions,[39,46] and both these reactions proceed via a CPET process. Given these limited examples, relatively little is known concerning the factors affecting the CPET, or, more broadly, PCET, reactions of mononuclear hydroxomanganese(III) species. This is despite several biological examples where Mn^{III}–OH units are involved in important oxidation/reduction reactions,[2,4,6,19] and stands in clear contrast to the abundance of studies focused on the PCET reactions of high-valent Mn-oxo and Mn-hydroxo species.[70,71] As noted by Mayer and coworkers, the oxidation reactions of lower-valent M^{II}/M^{III}

dx.doi.org/10.1021/ic500943k | Inorg. Chem. 2014, 53, 7622−7634

Scheme 2. Possible Pathways for PCET Reaction of $[Mn^{III}(OH)(dpaq)]^+$ with Phenols

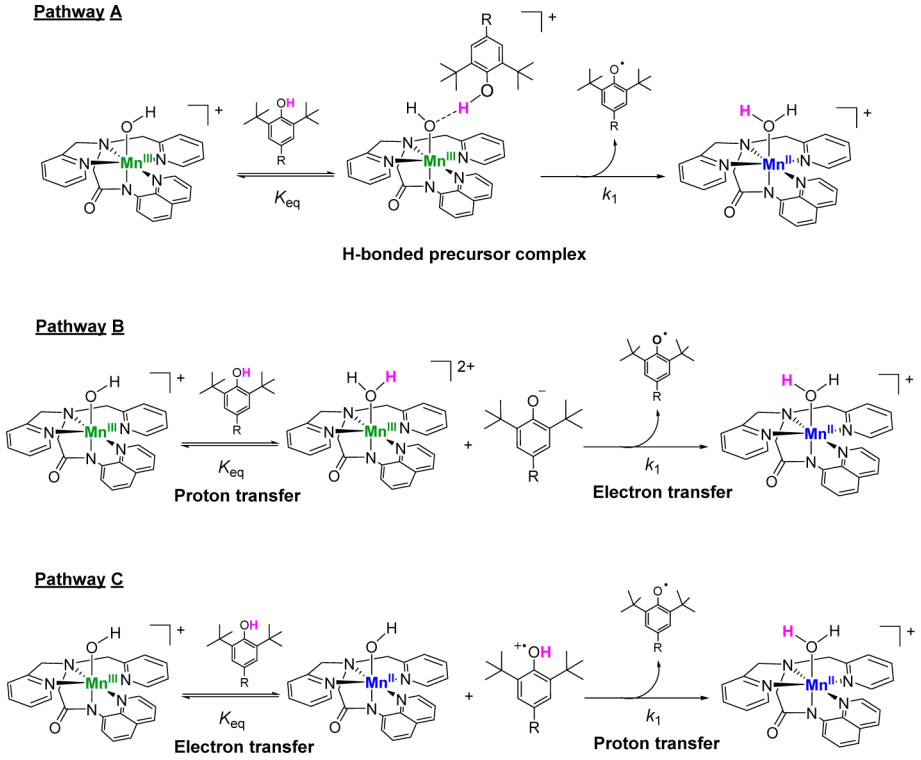

couples are overshadowed by studies of their high-valent counterparts.[72]

In this work, we have described a new mononuclear Mn^{III}–OH adduct, $[Mn^{III}(OH)(dpaq)]^+$, which is remarkably stable ($t_{1/2} \approx 26$ days at 25 °C in MeCN) and is formed in essentially quantitative yields from reaction of $[Mn^{II}(dpaq)](OTf)$ with O_2. Because of the high intrinsic reduction potential of the Mn^{III}/Mn^{II} couple, reactivity with O_2 is less common for manganese(II) centers when compared to analogous iron(II) centers.[73] To the best of our knowledge, the formation of $[Mn^{III}(OH)(S^{Me2}N_4(tren))]^+$ from O_2 and the corresponding Mn^{II} complex $[Mn^{II}(S^{Me2}N_4(tren))]^+$ represents the only other example of the quantative formation of a Mn^{III}–OH adduct from a Mn^{II} center and O_2.[46] In that case, a mono-oxo bridged dimanganese(III,III) complex served as an intermediate. Other examples of mononuclear Mn^{III}–OH adducts generated by O_2 oxidation of a Mn^{II} complex include $[Mn^{III}(OH)(OAc)(Me_2EBC)]^+$,[45] and a set of $[Mn^{III}(OH)(L)]^-$ species, where L is one of two trianionic tripodal ligands with a second-sphere cavity shielding the bound hydroxo ligand.[40,44] For one of the latter complexes, mechanistic studies provided evidence that the Mn^{III}–OH complex resulted from the initial formation of a peroxo-bridged-dimanganese(III,III) species that undergoes O–O bond homolysis to give two mononuclear Mn^{IV}=O intermediates.[44] The Mn^{IV}=O adducts convert to the observed Mn^{III}–OH species by a PCET reaction with solvent. More recently, Kovacs and co-workers have reported the first example of a peroxo-bridged-dimanganese(III,III) species, lending credence to this mechanism.[74] Investigations of the reaction of O_2 with the $[Mn^{II}(dpaq)](OTf)$ complex in MeCN using electronic absorption spectroscopy at low temperatures (−40 °C) provide no evidence for the formation of any intermediates en route to $[Mn^{III}(OH)(dpaq)]^+$. In addition, attempts to detect transient Mn^{IV}=O species have led to only negative results. For example, when the oxygenation of $[Mn^{II}(dpaq)](OTf)$ is carried out in the presence of 10 equiv PPh_3, the formation of O=PPh_3 is not observed and the yield of $[Mn^{III}(OH)(dpaq)]^+$ is unchanged. Nevertheless, the pathway for O_2-dependent formation of $[Mn^{III}(OH)(dpaq)]^+$ is currently under investigation, utilizing different solvent systems that may favor the formation of reaction intermediates.

$[Mn^{III}(OH)(dpaq)]^+$ is capable of oxidizing substrates with O–H BDFEs of <79 kcal/mol. Saturation behavior was observed in oxidation reactions with phenolic substrates. This is only the second report of a mononuclear Mn^{III}–OH adduct that is capable of performing a CPET reaction with phenols, and a relatively rare example of a Mn oxidant that shows saturation behavior in reaction with substrates.[75,76] Catalytic oxidation of organic substrates using O_2 as terminal oxidant is another attractive property of $[Mn^{III}(OH)(dpaq)]^+$, which is observed to perform over 1050 turnovers of TEMPOH in 3 h under the conditions employed. This turnover number is over 2 orders of magnitude larger than that observed for catalytic TEMPOH oxidation by $[Mn^{III}(OH)(S^{Me2}N_4(tren))]^+$,[46] although the catalytic activity for that system was not optimized.

Nature of Intermediate in Phenol Oxidation Reactions of $[Mn^{III}(OH)(dpaq)]^+$. PCET reactions can occur via a sequential pathway (i.e., initial proton transfer followed by electron transfer or vice versa) or a concerted pathway (CPET or HAT; see ref 16). The previously reported $[Mn^{III}(OH)(PY5)]^{2+}$ and $[Mn^{III}(OH)(S^{Me2}N_4(tren))]^+$ complexes (Figure 1), perform C–H and/or O–H bond oxidations by a CPET process, where the proton and electron are transferred in a single kinetic step.[39,46] In contrast, a mononuclear Mn^{III}-oxo complex, $[Mn^{III}(O)(H_3buea)]^{2-}$ (H_3buea = tris[(*N*′-*t*-butylureaylato)-*N*-ethyl]aminato), featuring a trianionic supporting ligand with a second-sphere hydrogen-bonding cavity around

dx.doi.org/10.1021/ic500943k | Inorg. Chem. 2014, 53, 7622–7634

Table 3. Reaction Parameters for Oxidation of TEMPOH by Hydroxometal(III) Adducts

complex	concentration (mM)	k_2 (M^{-1} s^{-1})	T (°C)	solvent	$\Delta H^{\ddagger}$ (kcal/mol)	$\Delta S^{\ddagger}$ (cal/(mol K))	$\Delta G^{\ddagger}$ (kcal/mol)
$[Mn^{III}(OH)(dpaq)]^+$	1.25	$1.3(1) \times 10^{-1}$	25	MeCN	9.9(9)	−35(3)	20.3
$[Mn^{III}(OH)(S^{Me2}N_4(tren))]^{+a}$	0.5	2.1×10^3	25	MeCN	8.2	−25.5	15.6
$Fe^{III}(OH)(TMP)^b$	0.08	$7.6(5) \times 10^1$	25	toluene	NR[c]	NR[c]	15.0(1)

[a]Data taken from ref 46. [b]Data taken from ref 72. [c]Not reported.

the oxo, performs C−H bond oxidation of dihydroanthracene through a sequential mechanism, with rate-limiting proton transfer prior to electron transfer.[66] This sequential pathway is favored for the Mn^{III}-oxo because of its high basicity (the pK_a of the corresponding Mn^{III}-hydroxo is 28.3 in DMSO[66]). In fact, treatment of $[Mn^{III}(O)(H_3buea)]^{2-}$ with $^{4\text{-}t\text{-butyl}}$ArOH in dimethylacetamide solvent resulted in a proton transfer reaction; oxidation of $^{4\text{-}t\text{-butyl}}$ArOH was not observed.[60]

The saturation behavior in the PCET reaction of $[Mn^{III}(OH)(dpaq)]^+$ with phenols could imply a sequential mechanism, as the kinetic behavior indicates an initial equilibration to an intermediate species prior to rate-determining formation of $[Mn^{II}(OH_2)(dpaq)]^+$ and the phenoxyl radical. In principle, there are several pathways consistent with saturation behavior, as outlined in Scheme 2. Pathway C, involving initial electron transfer, can be excluded on the basis of the unfavorability of oxidizing the ArOH substrates in the absence of their deprotonation, as well as the low $E_{1/2}$ value for $[Mn^{III}(OH)(dpaq)]^+$ (vide supra).[48]

There are several lines of evidence that the equilibrium step does not involve an initial proton transfer but potentially involves the formation of a hydrogen-bonded complex (pathways B and A, respectively; see Scheme 2). First, there is no correlation between the observed K_{eq} values and the pK_a values of the phenols (Table 2). A correlation would be expected if the equilibrium were due to a proton transfer from the phenol to $[Mn^{III}(OH)(dpaq)]^+$.[77] Second, the electronic absorption spectrum of the intermediate, obtained within 0.5 s of adding a large excess of $^{4\text{-}t\text{-butyl}}$ArOH to a MeCN solution of $[Mn^{III}(OH)(dpaq)]^+$, is almost identical to that of $[Mn^{III}(OH)(dpaq)]^+$ (Figure S6 in the Supporting Information). Although the electronic absorption spectrum of a putative $[Mn^{III}(OH_2)(dpaq)]^{2+}$ species is not known, it is reasonable to assume that the change from hydroxo to aqua ligation would significantly perturb the ligand-field splitting of the Mn^{III} center (potentially causing a reorientation of the pseudo-Jahn−Teller axis[78]), resulting in noticeable shifts of the d−d transition energies. The minor changes observed experimentally are more consistent with a hydrogen-bonding interaction.[79] Third, the KIE of 1.4 for the rate-determining step in the reaction of $[Mn^{III}(OH)(dpaq)]^+$ with $^{4\text{-}t\text{-butyl}}$ArOH suggests that phenol O−H bond breaking be part of this step. Finally, k_1 is related to the BDFE values of the phenol O−H bonds, which is a hallmark of a CPET process. Given the above considerations, we conclude that the initial equilibrium step features the formation of a precursor complex, likely stabilized by hydrogen-bonding interactions, and that the rate-determining step is a CPET.

When CPET reactions are considered within the framework of Marcus theory, a precursor (or encounter) complex is expected to form prior to rate-determining proton−electron transfer.[80] While rare, precursor complexes have been observed for other CPET processes, and these are often,[75,81,82] but not always,[76] mediated by hydrogen-bonding interactions with an O−H group on the substrate. For example, a Mn^{IV}-hydroxo adduct supported by a bulky salen derivative also showed saturation behavior in reactions with substituted phenols.[75,76] For the reaction with $^{4\text{-H}}$ArOH, in particular, a K_{eq} of ∼5000 was determined, and this equilibrium was attributed to the formation of a hydrogen-bonded complex. No initial equilibrium was observed in the reaction of the corresponding Mn^{IV}-oxo adduct with phenols.[75,76] In addition, Costas and co-workers observed the formation of a precursor complex in the reaction of hydrocarbons with an oxohydroxomanganese(IV) moeity supported by a neutral N_4 ligand, but the forces stabilizing the precursor complex remain unclear.[76] Saturation behavior was not observed in analogous reactions with the corresponding di(hydroxo)manganese(IV) complex. Taken together, these prior studies demonstrate that subtle changes in properties of the metal-based oxidant can dramatically affect whether or not the formation of a precursor complex is observed.

Nevertheless, it is somewhat curious that saturation behavior should be observed in the reaction of $[Mn^{III}(OH)(dpaq)]^+$ with phenols, but not with TEMPOH, which likewise contains an O−H unit capable of hydrogen bonding. Indeed, TEMPOH has been shown to form a hydrogen-bond-mediated precursor complex, prior to rate-liming CPET, with $[Co^{III}(Hbim)(H_2bim)_2]^{2+}$ (H_2bim = 2,2′-biimidazoline).[79] However, given that the K_{eq} values observed for reaction of $[Mn^{III}(OH)(dpaq)]^+$ with phenols reflect small stabilizations in terms of free energy (−4.2 kcal/mol to −1.3 kcal/mol), seemingly minor differences in the hydrogen-bond donating (or accepting) ability of the phenol versus TEMOPH substrates, and/or changes in solvent reorganization energies upon precursor complex formation, could lead to a precursor complex being less favorable in the case of TEMPOH substrate. Taken together, this and other work highlights our nascent understanding of the optimal conditions that must be achieved to observe formation of a precursor complex, and the impacts of precursor complexes on the overall CPET process.[75,76,81,82]

CPET Reactivity of Mononuclear Mn^{III}−OH Complexes. To the best of our knowledge, $[Mn^{III}(OH)(dpaq)]^+$ is only the third hydroxomanganese(III) complex known to facilitate either O−H or C−H bond oxidations. As both $[Mn^{III}(OH)(dpaq)]^+$ and $[Mn^{III}(OH)(S^{Me2}N_4(tren))]^+$ (Figure 1, right) react with TEMPOH at 25 °C in MeCN, a direct comparison can be made between these oxidants. Based on these kinetic data, $[Mn^{III}(OH)(S^{Me2}N_4(tren))]^+$ is a more rapid oxidant,[46] showing a second-order rate constant for TEMPOH oxidation 10^4-fold larger than that of $[Mn^{III}(OH)(dpaq)]^+$ (see Table 3). The faster reaction for $[Mn^{III}(OH)(S^{Me2}N_4(tren))]^+$ is a consequence of a smaller enthalpy *and* entropy of activation compared to $[Mn^{III}(OH)(dpaq)]^+$ (Table 3). In both systems the negative $\Delta S^{\ddagger}$ values mark an associative process; the substantially more negative $\Delta S^{\ddagger}$ for the reaction involving $[Mn^{III}(OH)(dpaq)]^+$ implies a more ordered transition state. The smaller $\Delta H^{\ddagger}$ for the reaction of $[Mn^{III}(OH)(S^{Me2}N_4(tren))]^+$ is tentatively attributed to an increased nucleophilicity caused by the electron-donating thiolate ligand.

dx.doi.org/10.1021/ic500943k | Inorg. Chem. 2014, 53, 7622−7634

A similar effect has been observed in CPET reactions of a thiolate-ligated oxoiron(IV) complex.[83] Also of relevance in comparing TEMPOH reactivity with metal-hydroxo adducts is a recent study of the hydroxoiron(III) complex $Fe^{III}(OH)$-(TMP), which features a tetramesitylporphyrin supporting ligand.[72] In that case, a second-order rate constant of 76(5) M^{-1} s^{-1} was observed for the oxidation of TEMPOH at 25 °C in toluene (Table 3).

Although both $[Mn^{III}(OH)(S^{Me2}N_4(tren))]^+$ and $Fe^{III}(OH)$-(TMP) react with TEMPOH much more rapidly than $[Mn^{III}(OH)(dpaq)]^+$, neither of those complexes is able to oxidize substrates with larger BDFEs. For example, $Fe^{III}(OH)$-(TMP) showed no reaction with $^{4\text{-}t\text{-butyl}}$ArOH over a period of 24 h,[72] and the normal decay rate of $[Mn^{III}(OH)$-$(S^{Me2}N_4(tren))]^+$ was unaffected by the presence of a large excess of 1,4-cyclohexadience, dihydroanthracene, or toluene.[46] In contrast, $[Mn^{III}(OH)(dpaq)]^+$ reacts with phenols with O−H BDFEs up to 79 kcal/mol, and can also activate the weak C−H bonds of xanthene (BDFE = 73.3 kcal/mol in dimethyl sulfoxide). $[Mn^{III}(OH)(dpaq)]^+$ reacts with a large excess (250 equiv) of xanthene with a pseudo-first-order rate constant of 8 × 10^{-4} s^{-1} at 50 °C in MeCN, which is an order of magnitude slower than that observed for $[Mn^{III}(OH)(PY5)]^{2+}$,[39] the only other Mn^{III}−OH complex known to oxidize C−H bonds.

For the reaction of $[Mn^{III}(OH)(dpaq)]^+$ with phenols, the rate of reaction is only weakly dependent on the phenol O−H BDFE (Figure 10). In particular, the observed slope of the log(k) versus BDFE correlation is only −0.07, which is significantly lower than the expected Marcus theory value of −0.5 for a reaction with a small thermodynamic driving force.[80] However, this slope should be viewed within the caveat that the linear-free energy relationship is only for a small range of substrate BDFEs. In any case, values between −0.5 and −0.3 have been reported for transition-metal oxidants,[80,84] including oxoruthenium(IV)[85] and oxomanganese(IV)[70,76] species, and are commonly interpreted as implying a symmetric transition state structure. Notably, a similarly weak correlation between rate and substrate BDE was observed for hydrocarbon oxidation by $[Mn^{III}(OH)(PY5)]^{2+}$ (slope = −0.1), and this was attributed to unusually large reorganizational energies of the oxidant ($\Delta S^{\ddagger}$ = −36(5) cal/(mol K) for the reaction of $[Mn^{III}(OH)(PY5)]^{2+}$ with dihydroanthracene).[39] This interpretation would be consistent with other instances were small slopes have been attributed to large entropies of reorganization, such that $T\Delta S^{\ddagger} > \Delta H^{\ddagger}$.[82]

It is tempting to speculate on whether the low dependence of the reaction rate on the substrate BDFE is a general feature of CPET reactions by manganese(III) centers that could be related to relatively large entropies of activation. This of course would have implications for the suitability of such oxidants in synthetic and biological oxidation reactions and/or bear relevance to the mechanisms by which protein active sites tune the geometric and electronic structure to minimize reorganization during CPET. However, to the best of our knowledge, the set of reactions of $[Mn^{III}(OH)(dpaq)]^+$ and $[Mn^{III}(OH)(PY5)]^{2+}$ with phenols and hydrocarbons, respectively, provide the only examples of linear-free energy relationships for CPET by manganese(III) centers. It is, therefore, ill-advised to draw far-reaching conclusions from this limited dataset. Nonetheless, this work reveals complexities in identifying the geometric and electronic factors that contribute to the kinetic and thermodynamic behavior of PCET reactions and illustrates the importance of extending detailed studies of such reactions to mid- and even low-valent transition-metal oxidants.

■ ASSOCIATED CONTENT

Ⓢ Supporting Information

Crystal data and structure refinement tables for $[Mn^{II}(dpaq)]$-(OTf) and $[Mn^{III}(OH)(dpaq)](OTf)$; ESI-MS plots; yields of $^{4\text{-}t\text{-butyl}}$ArO• from $^{4\text{-}t\text{-butyl}}$ArOH oxidation by $[Mn^{III}(OH)$-$(dpaq)]^+$; X-band EPR data for $[Mn^{II}(dpaq)](OTf)$, $[Mn^{III}(OH)(dpaq)](OTf)$ and oxidation reaction products; cyclic voltammetry data for $[Mn^{III}(OH)(dpaq)]^+$; kinetic data for reactions of $[Mn^{III}(OH)(dpaq)]^+$ with xanthene and substituted phenols; electronic absorption spectra of $[Mn^{III}(OH)(dpaq)]^+$ immediately following the addition of a large excess of $^{4\text{-}t\text{-butyl}}$ArOH; results of catalytic TEMPOH oxidation by $[Mn^{II}(dpaq)](OTf)$. This material is available free of charge via the Internet at http://pubs.acs.org.

■ AUTHOR INFORMATION

Corresponding Author

*Tel.: (785) 864-3968. Fax: (785) 864-5396 taj@ku.edu.

Notes

The authors declare no competing financial interest.

■ ACKNOWLEDGMENTS

This work was supported by the U.S. National Science Foundation (No. CHE-1056470 to T.A.J.). B.C. was supported by funds from an NSF-Research Experience for Undergraduate program (No. CHE-1004897). The U.S. National Science Foundation is also acknowledged for funds used for the purchase of X-ray instruments (No. CHE-0079282) and the EPR spectrometer (No. CHE-0946883). Prof. Mikhail Barybin and Dr. John Meyers Jr. are acknowledged for their generous assistance in the collection and interpretation of the electrochemical data.

■ REFERENCES

(1) Cotruvo, J. J. A.; Stubbe, J. *Metallomics* **2012**, *4*, 1020−1036.
(2) McEvoy, J. P.; Brudvig, G. W. *Chem. Rev. (Washington, DC, U. S.)* **2006**, *106*, 4455−4483.
(3) Miller, A.-F. *Curr. Opin. Chem. Biol.* **2004**, *8*, 162−168.
(4) Grove, L. E.; Brunold, T. C. *Comments Inorg. Chem.* **2008**, *29*, 134−168.
(5) Su, C.; Oliw, E. H. *J. Biol. Chem.* **1998**, *273*, 13072−13079.
(6) Su, C.; Sahlin, M.; Oliw, E. H. *J. Biol. Chem.* **2000**, *275*, 18830−18835.
(7) Miller, A.-F.; Padmakumar, F.; Sorkin, D.; Karapetian, A.; Vance, C. K. *J. Inorg. Biochem.* **2003**, *93*, 71−83.
(8) Han, W.-G.; Lovell, T.; Noodleman, L. *Inorg. Chem.* **2002**, *41*, 205−218.
(9) Jackson, T. A.; Gutman, C. T.; Maliekal, J.; Miller, A.-F.; Brunold, T. C. *Inorg. Chem.* **2013**, *52*, 3356−3367.
(10) Vance, C. K.; Miller, A.-F. *J. Am. Chem. Soc.* **1998**, *120*, 461−467.
(11) Vance, C. K.; Miller, A. F. *Biochemistry* **2001**, *40*, 13079−13087.
(12) Jackson, T. A.; Brunold, T. C. *Acc. Chem. Res.* **2004**, *37*, 461−470.
(13) Although Mn-lipoxygenase has not been structurally characterized, the presence of a monuclear $Mn^{III}(OH)$ unit is inferred on the basis of analogy to the active site of Fe-lipoxygenase; see Boyington, J.; Gaffney, B.; Amzel, L. *Science* **1993**, *260*, 1482−1486. Minor, W.; Steczko, J.; Stec, B.; Otwinowski, Z.; Bolin, J. T.; Walter, R.; Axelrod, B. *Biochemistry* **1996**, *35*, 10687−10701.
(14) Umena, Y.; Kawakami, K.; Shen, J.-R.; Kamiya, N. *Nature (London, U. K.)* **2011**, *473*, 55−60.

(15) Pal, R.; Negre, C. F. A.; Vogt, L.; Pokhrel, R.; Ertem, M. Z.; Brudvig, G. W.; Batista, V. S. *Biochemistry* **2013**, *52*, 7703−7706.
(16) In this work, we use PCET to refer broadly to any reaction involving the overall transfer of a proton and an electron. Consequently, PCET reactions can occur in a sequential manner, where the electron and proton are transferred in separate kinetic steps, or can occur in a concerted process. Concerted processes can be further described as hydrogen-atom transfer (HAT) or concerted proton−electron transfer (CPET). HAT is often invoked when the proton and electron are transferred to the same orbital or bond, whereas CPET is used to describe cases where the electron and proton are transferred to separate orbitals and/or bonds. With this definition, CPET is common for transition metal-oxo or -hydroxo species, where the electron is transferred to the metal and the proton is transferred to the oxo or hydroxo ligand. A more rigorous distinction between HAT and CPET has been offered by Hammes-Shiffer and co-workers (see ref 17), and depends on whether the proton transfer is electronically adiabatic (HAT) or nonadiabatic (CPET).
(17) Layfield, J. P.; Hammes-Schiffer, S. *Chem. Rev. (Washington, DC, U. S.)* **2013**, *114*, 3466−3494.
(18) The k_H/k_D value was temperature-independent over the measured range of 5−45 °C.
(19) Mullins, C. S.; Pecoraro, V. L. *Coord. Chem. Rev.* **2008**, *252*, 416−443.
(20) Tommos, C.; Babcock, G. T. *Acc. Chem. Res.* **1998**, *31*, 18−25.
(21) Tang, X.-S.; Randall, D. W.; Force, D. A.; Diner, B. A.; Britt, R. D. *J. Am. Chem. Soc.* **1996**, *118*, 7638−7639.
(22) Siegbahn, P. E. M. *Inorg. Chem.* **2000**, *39*, 2923−2935.
(23) Zouni, A.; Witt, H.-T.; Kern, J.; Fromme, P.; Krauss, N.; Saenger, W.; Orth, P. *Nature (London, U.K.)* **2001**, *409*, 739−743.
(24) Gilchrist, M. L.; Ball, J. A.; Randall, D. W.; Britt, R. D. *Proc. Natl. Acad. Sci. U. S. A.* **1995**, *92*, 9545−9549.
(25) Hoganson, C.; Lydakis-Simantiris, N.; Tang, X.-S.; Tommos, C.; Warncke, K.; Babcock, G.; Diner, B.; McCracken, J.; Styring, S. *Photosynth. Res.* **1995**, *46*, 177−184.
(26) Babcock, G. T. In *Photosynthesis: From Light to Biosphere*; Kluwer: Dordrecht, The Netherlands, 1995; Vol. *2*, pp 209−215.
(27) Baldwin, M. J.; Pecoraro, V. L. *J. Am. Chem. Soc.* **1996**, *118*, 11325−11326.
(28) Caudle, M. T.; Pecoraro, V. L. *J. Am. Chem. Soc.* **1997**, *119*, 3415−3416.
(29) Wang, K.; Mayer, J. M. *J. Am. Chem. Soc.* **1997**, *119*, 1470−1471.
(30) Bordwell, F. G.; Cheng, J. *J. Am. Chem. Soc.* **1991**, *113*, 1736−1743.
(31) Larsen, A. S.; Wang, K.; Lockwood, M. A.; Rice, G. L.; Won, T.-J.; Lovell, S.; Sadílek, M.; Tureček, F.; Mayer, J. M. *J. Am. Chem. Soc.* **2002**, *124*, 10112−10123.
(32) Mukhopadhyay, S.; Mandal, S. K.; Bhaduri, S.; Armstrong, W. H. *Chem. Rev. (Washington, DC, U. S.)* **2004**, *104*, 3981−4026.
(33) Sano, Y.; Weitz, A. C.; Ziller, J. W.; Hendrich, M. P.; Borovik, A. S. *Inorg. Chem.* **2013**, *52*, 10229−10231.
(34) Baldwin, M. J.; Law, N. A.; Stemmler, T. L.; Kampf, J. W.; Penner-Hahn, J. E.; Pecoraro, V. L. *Inorg. Chem.* **1999**, *38*, 4801−4809.
(35) Baldwin, M. J.; Stemmler, T. L.; Riggs-Gelasco, P. J.; Kirk, M. L.; Penner-Hahn, J. E.; Pecoraro, V. L. *J. Am. Chem. Soc.* **1994**, *116*, 11349−11356.
(36) Zhou, H.-B.; Wang, H.-S.; Chen, Y.; Xu, Y.-L.; Song, X.-J.; Song, Y.; Zhang, Y.-Q.; You, X.-Z. *Dalton Trans.* **2011**, *40*, 5999−6006.
(37) Park, Y. J.; Ziller, J. W.; Borovik, A. S. *J. Am. Chem. Soc.* **2011**, *133*, 9258−9261.
(38) Cheng, B.; Fries, P. H.; Marchon, J.-C.; Scheidt, W. R. *Inorg. Chem.* **1996**, *35*, 1024−1032.
(39) Goldsmith, C. R.; Cole, A. P.; Stack, T. D. P. *J. Am. Chem. Soc.* **2005**, *127*, 9904−9912.
(40) Shirin, Z.; Hammes, B. S.; Young, V. G.; Borovik, A. S. *J. Am. Chem. Soc.* **2000**, *122*, 1836−1837.
(41) El Ghachtouli, S.; Lassalle-Kaiser, B.; Dorlet, P.; Guillot, R.; Anxolabéhère-Mallart, E.; Costentin, C.; Aukauloo, A. *Energy Environ. Sci.* **2011**, *4*, 2041−2044.
(42) Eroy-Reveles, A. A.; Leung, Y.; Beavers, C. M.; Olmstead, M. M.; Mascharak, P. K. *J. Am. Chem. Soc.* **2008**, *130*, 4447−4458.
(43) Eichhorn, D. M.; Armstrong, W. H. *J. Chem. Soc., Chem. Commun.* **1992**, 85−87.
(44) Shirin, Z.; Borovik, A. S.; Young, V. G., Jr. *Chem. Commun. (Cambridge, U.K.)* **1997**, 1967−1968.
(45) Hubin, T. J.; McCormick, J. M.; Alcock, N. W.; Busch, D. H. *Inorg. Chem.* **2001**, *40*, 435−444.
(46) Coggins, M. K.; Brines, L. M.; Kovacs, J. A. *Inorg. Chem.* **2013**, *52*, 12383−12393.
(47) Shook, R. L.; Peterson, S. M.; Greaves, J.; Moore, C.; Rheingold, A. L.; Borovik, A. S. *J. Am. Chem. Soc.* **2011**, *133*, 5810−5817.
(48) Warren, J. J.; Tronic, T. A.; Mayer, J. M. *Chem. Rev. (Washington, DC, U. S.)* **2010**, *110*, 6961−7001.
(49) Hitomi, Y.; Iwamoto, Y.; Kodera, M. *Dalton Trans.* **2014**, *43*, 2161−2167.
(50) Hitomi, Y.; Arakawa, K.; Funabiki, T.; Kodera, M. *Angew. Chem., Int. Ed.* **2012**, *51*, 3448−3452.
(51) Coggins, M. K.; Zhang, M.-T.; Vannucci, A. K.; Dares, C. J.; Meyer, T. J. *J. Am. Chem. Soc.* **2014**, *136*, 5531−5534.
(52) Wu, A.; Mader, E. A.; Datta, A.; Hrovat, D. A.; Borden, W. T.; Mayer, J. M. *J. Am. Chem. Soc.* **2009**, *131*, 11985−11997.
(53) Lansky, D. E.; Goldberg, D. P. *Inorg. Chem.* **2006**, *45*, 5119−5125.
(54) Seo, M. S.; Kim, J. Y.; Annaraj, J.; Kim, Y.; Lee, Y.-M.; Kim, S.-J.; Kim, J.; Nam, W. *Angew. Chem., Int. Ed. Engl.* **2007**, *46*, 377−380.
(55) Evans, D. F.; Jakubovic, D. A. *J. Chem. Soc., Dalton Trans.* **1988**, 2927−2933.
(56) *Refinement: SHELXTL v2010.3−0*; Bruker-AXS, E.C.P.: Madison, WI.
(57) *International Tables for Crystallography*, Vol. *A*, 4th Edition; Kluwer: Boston, 1996.
(58) *Data Collection: SMART Software in APEX2 v2010.3−0 Suite*; Bruker-AXS, E.C.P.: Madison, WI.
(59) *Data Reduction: SAINT Software in APEX2 v2010.3−0 Suite*; Bruker-AXS, E.C.P.: Madison, WI.
(60) Gupta, R.; Borovik, A. S. *J. Am. Chem. Soc.* **2003**, *125*, 13234−13242.
(61) Ottaviani, M. F.; Garcia-Garibay, M.; Turro, N. J. *Colloids Surf., A* **1993**, *72*, 321−332.
(62) Manner, V. W.; Lindsay, A. D.; Mader, E. A.; Harvey, J. N.; Mayer, J. M. *Chem. Sci.* **2012**, *3*, 230−243.
(63) Manner, V. W.; Markle, T. F.; Freudenthal, J. H.; Roth, J. P.; Mayer, J. M. *Chem. Commun. (Cambridge, U.K.)* **2008**, 256−258.
(64) Waidmann, C. R.; Zhou, X.; Tsai, E. A.; Kaminsky, W.; Hrovat, D. A.; Borden, W. T.; Mayer, J. M. *J. Am. Chem. Soc.* **2009**, *131*, 4729−4743.
(65) Kütt, A.; Leito, I.; Kaljurand, I.; Sooväli, L.; Vlasov, V. M.; Yagupolskii, L. M.; Koppel, I. A. *J. Org. Chem.* **2006**, *71*, 2829−2838.
(66) Parsell, T. H.; Yang, M.-Y.; Borovik, A. S. *J. Am. Chem. Soc.* **2009**, *131*, 2762−2763.
(67) Lassalle-Kaiser, B.; Hureau, C.; Pantazis, D. A.; Pushkar, Y.; Guillot, R.; Yachandra, V. K.; Yano, J.; Neese, F.; Anxolabehere-Mallart, E. *Energy Environ. Sci.* **2010**, *3*, 924−938.
(68) Gupta, R.; Taguchi, T.; Borovik, A. S.; Hendrich, M. P. *Inorg. Chem.* **2013**, *52*, 12568−12575.
(69) Borovik, A. S. *Acc. Chem. Res.* **2004**, *38*, 54−61.
(70) Leto, D. F.; Ingram, R.; Day, V. W.; Jackson, T. A. *Chem. Commun. (Cambridge, U.K.)* **2013**, *49*, 5378−5380.
(71) Wang, Y.; Shi, S.; Wang, H.; Zhu, D.; Yin, G. *Chem. Commun. (Cambridge, U.K.)* **2012**, *48*, 7832−7834.
(72) Porter, T. R.; Mayer, J. M. *Chem. Sci.* **2014**, *5*, 372−380.
(73) Rybak-Akimova, E. V. In *Physical Inorganic Chemistry: Reactions, Processes, and Applications*; Bakac, A., Ed.; John Wiley & Sons, Inc.: Hoboken, NJ, 2010; pp 109−188.
(74) Coggins, M. K.; Sun, X.; Kwak, Y.; Solomon, E. I.; Rybak-Akimova, E.; Kovacs, J. A. *J. Am. Chem. Soc.* **2013**, *135*, 5631−5640.
(75) Kurahashi, T.; Kikuchi, A.; Shiro, Y.; Hada, M.; Fujii, H. *Inorg. Chem.* **2010**, *49*, 6664−6672.

(76) Garcia-Bosch, I.; Company, A.; Cady, C. W.; Styring, S.; Browne, W. R.; Ribas, X.; Costas, M. *Angew. Chem., Int. Ed. Engl.* **2011**, *50*, 5648−5653.
(77) It would also appear reasonable to anticipate a relationship between the pK_a of the phenol and the equilibrium constant for the formation of a hydrogen-bonded complex, when the phenol is the hydrogen-bond donor. In contrast, if the Mn^{III}−OH unit were to serve as a hydrogen-bond donor, then no correlation between pK_a and the K_{eq} values would be expected. In that scenario, rapid hydrogen-bond rearrangement would be required prior to rate-limiting CPET.
(78) Jackson, T. A.; Karapetian, A.; Miller, A.-F.; Brunold, T. C. *J. Am. Chem. Soc.* **2004**, *126*, 12477−12491.
(79) Mader, E. A.; Mayer, J. M. *Inorg. Chem.* **2010**, *49*, 3685−3687.
(80) Mayer, J. M. *Acc. Chem. Res.* **2010**, *44*, 36−46.
(81) Kojima, T.; Hirai, Y.; Ishizuka, T.; Shiota, Y.; Yoshizawa, K.; Ikemura, K.; Ogura, T.; Fukuzumi, S. *Angew. Chem., Int. Ed. Engl.* **2010**, *49*, 8449−8453.
(82) Ishizuka, T.; Ohzu, S.; Kotani, H.; Shiota, Y.; Yoshizawa, K.; Kojima, T. *Chem. Sci.* **2014**, *5*, 1429−1436.
(83) Sastri, C. V.; Lee, J.; Oh, K.; Lee, Y. J.; Lee, J.; Jackson, T. A.; Hirao, H.; Que, L., Jr.; Shaik, S.; Nam, W. *Proc. Natl. Acad. Sci. U. S. A.* **2007**, *104*, 19181−19186.
(84) Gardner, K. A.; Kuehnert, L. L.; Mayer, J. M. *Inorg. Chem.* **1997**, *36*, 2069−2078.
(85) Matsuo, T.; Mayer, J. M. *Inorg. Chem.* **2005**, *44*, 2150−2158.